Supplement of Atmos. Meas. Tech., 18, 773–792, 2025
https://doi.org/10.5194/amt-18-773-2025-supplement

Atmospheric Measurement Techniques
Open Access
EGU

Supplement of

Retrieving cloud-base height and geometric thickness using the oxygen A-band channel of GCOM-C/SGLI

Takashi M. Nagao et al.

Correspondence to: Takashi M. Nagao (tmnagao@aori.u-tokyo.ac.jp)

Text S1. Forward model for visible, near-infrared, and shortwave-infrared channels

In this study, the satellite-observed TOA reflectance computations $R_{toa,crg}$ which incorporate cloud scattering, Rayleigh scattering, and gas absorption in the cloud retrieval algorithms employed the following approximate representations (S1–S9) developed based on techniques from previous studies (Nakajima and Nakajima, 1995; Walther and Heidinger, 2012; Hayashi, 2018). Table S1 provides the notations of the symbols in equations (S1–S9) along with the meanings of the superscripts and subscripts. Table S2 provides the variables related to geometry, pressure, cloud property, and gaseous scattering and absorption on which each component of equations (S1–S9) depends.

$$R_{toa,crg} = T_{ac,g}^{\downarrow} T_{ac,g}^{\uparrow} R_{toc,crg} \,, \tag{S1}$$

$$R_{toc,crg} = R_{bd} + \frac{\left(T_{cr}^{\downarrow} T_{cr}^{\uparrow}\right)\left(T_{bc,g}^{\downarrow} T_{bc,g}^{\uparrow}\right) A_s}{1 - \left(T_{bc,g}^{\downarrow} T_{bc,g}^{\uparrow}\right) A_s R_{sa,cr}} \,, \tag{S2}$$

$$R_{bd} = \begin{cases} R_{bd,cr} \,, & \text{except VN9} \\ R_{bd,crg} \,, & \text{for VN9} \end{cases} . \tag{S3}$$

The term $R_{bd,crg}$ in equation S3 was introduced in this study; whereas, Nagao and Suzuki (2021) uses $R_{bd,cr}$, assuming cloud geometric thickness to be zero and neglecting in-cloud gas absorption, $R_{bd,cr}$ consider them to simulate reflectance at oxygen A-band channel (SGLI VN9). Each variable in equations S1 and S2 is written as follows: many include both the cloud top pressure P_c and surface pressure P_s because they consider the interaction between Rayleigh scattering and gaseous absorption. To reduce the dimensionality of the look-up table, the following representations (S4–S8) separate the P_c and P_s where possible:

$$R_{bd,cr}(P_c, P_s) = R_{bd,cr}(P_0, P_0) + T_c^{\downarrow} T_c^{\uparrow} \{R_{bc,r}(P_s) - R_{bc,r}(P_0)\} \,, \tag{S4}$$

$$R_{sa,cr}(P_c, P_s) = R_{sa,cr}(P_0, P_0) + \{R_{sa,r}(P_s) - R_{sa,r}(P_0)\} \,, \tag{S5}$$

$$T_{cr}^{\downarrow(\uparrow)}(P_c, P_s) = T_{cr}^{\downarrow(\uparrow)}(P_0, P_0) \frac{T_r^{\downarrow(\uparrow)}(P_s)}{T_r^{\downarrow(\uparrow)}(P_0)} \,, \tag{S6}$$

$$T_{ac,g}^{\downarrow(\uparrow)}(P_c) = T_g^{\downarrow(\uparrow)}(P_c) \,, \tag{S7}$$

$$T_{bc,g}^{\downarrow(\uparrow)}(P_c, P_s) = \frac{T_g^{\downarrow(\uparrow)}(P_s)}{T_{ac,g}^{\downarrow(\uparrow)}(P_c)} \,. \tag{S8}$$

Additionally, water vapor (H_2O), carbon dioxide (CO_2), ozone (O_3), oxygen (O_2), and other gases (others) were considered for the total gas absorption.

$$T_g^{\downarrow(\uparrow)}(P) = T_{g,H_2O}^{\downarrow(\uparrow)}(P) T_{g,CO_2}^{\downarrow(\uparrow)}(P) T_{g,CO_2}^{\downarrow(\uparrow)}(P) T_{g,O_3}^{\downarrow(\uparrow)}(P) T_{g,O_2}^{\downarrow(\uparrow)}(P) T_{g,others}^{\downarrow(\uparrow)}(P) \,. \tag{S9}$$

In this study, we used a multilayer perceptron (MLP) with two hidden layers, a type of artificial neural networks (NNs), instead of a typical LUT with polynomial approximations in the retrieval process. One advantage of using MLP is that precomputed points can be defined at unequal intervals and that memory use can be reduced compared to the usual LUT approach for an increased number of explanatory variables. Table S3 shows the precomputed points for the NN-based LUTs used in this study.

Table S1. Notations of symbols in equations (S1–S9).

Superscript		Descriptions
$\downarrow$ / $\uparrow$		Downward / Upward
Subscript		
c		Considering scattering by cloud particle
r		Considering Rayleigh scattering by air molecules
g		Considering gas absorption
cr		Considering scattering by cloud particle and air molecules
crg		Considering scattering by cloud particle and air molecules and gas absorption
toa / toc		At top of atmosphere / At top of cloud
ac / bc		Above cloud / Below cloud
Variables	**Variables with super- and subscripts**	
R	$R_{toa,crg}$	Reflectance at top of atmosphere for [crg]
	$R_{toc,crg}$	- at top of cloud
R_{bd}	$R_{bd,[c,r,cr,crg]}$	Bidirectional reflectance scattered to sensor for [c, r, cr, crg]
R_{sa}	$R_{sa,[c,r,cr]}$	Spherical albedo for [c, r, cr]
T	$T^{\downarrow(\uparrow)}{}_{[c,r,cr]}$	Downward (upward) transmittance function for [c, r, cr]
	$T^{\downarrow(\uparrow)}{}_{g}$	- through atmospheric gases
	$T^{\downarrow(\uparrow)}_{g,[H_2O,CO_2,O_3,O_2]}$	- through [water vapor, carbon dioxide, ozone, oxygen]
	$T_{g,other}$	- through the other gases including trace gases
A_s		Surface albedo

Table S2. Variables related to geometry, pressure, cloud property, and gaseous scattering and absorption (explanatory variables) considered for each component (object variables) of equations (S1–S9).

	Explanatory variable			
	Geometry	Pressure	Cloud property	Gas
	θ_0: solar zenith θ_1: sensor zenith Φ: relative azimuth	P_c: cloud top pressure P_b: cloud base pressure P_s : surface pressure	τ_c : optical thickness r_e : effective radius $ICOTF$: $\tau_{ICE}/(\tau_{LIQ}+\tau_{ICE})$	TPW: total precipitable water for H_2O COL : column mean concentration for CO_2 DU : Dobson unit of O_3
Object variable	Depending on			
$R_{bd,cr}$	θ_0, θ_1, Φ	Fixed $P_c = P_0, P_s = P_0$	$\tau_c, r_e, ICOTF$	-
$R_{bd,crg}$	θ_0, θ_1, Φ	P_c, P_b, P_s	$\tau_c, r_e, ICOTF$	(VN9 only: considering in-cloud O_2 absorption)
$R_{bd,r}$	θ_0, θ_1, Φ	P_s	-	-
$R_{sa,cr}$	-	Fixed $P_c = P_0, P_s = P_0$	$\tau_c, r_e, ICOTF$	-
$R_{sa,r}$	-	P_s	-	-
$T_{cr}^{\downarrow(\uparrow)}$	$\theta_0, (\theta_1)$	Fixed $P_c = P_0, P_s = P_0$	$\tau_c, r_e, ICOTF$	-
$T_{c}^{\downarrow(\uparrow)}$	$\theta_0, (\theta_1)$	-	$\tau_c, r_e, ICOTF$	-
$T_{r}^{\downarrow(\uparrow)}$	$\theta_0, (\theta_1)$	P_s	-	-
$T_{g,H_2O}^{\downarrow(\uparrow)}$	$\theta_0, (\theta_1)$	P_s	-	TPW
$T_{g,CO_2}^{\downarrow(\uparrow)}$	$\theta_0, (\theta_1)$	P_s	-	COL
$T_{g,O_3}^{\downarrow(\uparrow)}$	$\theta_0, (\theta_1)$	P_s	-	DU
$T_{g,O_2}^{\downarrow(\uparrow)}$	$\theta_0, (\theta_1)$	P_s	-	-
$T_{g,others}^{\downarrow(\uparrow)}$	$\theta_0, (\theta_1)$	P_s	-	-

Table S3. Precomputed points of each variable used to train an artificial neural network.

Variable	Description	Unit	Precomputed points
θ_0	Solar zenith	deg.	0, …, 70 by 5
θ_1	Sensor zenith	deg.	0, …, 70 by 5
Φ	Relative azimuth	deg.	0, …, 180 by 10
P_c	Cloud top pressure	hPa	13.25, …, 1013.25 by 50
P_b	Cloud base pressure	hPa	13.25, …, 1013.25 by 50 $(P_s \leq P_b \leq P_c)$
P_s	Surface pressure	hPa	13.25, …, 1013.25 by 50
τ_c	Optical thickness	-	0.0, 0.1, 0.25, 0.5, 1.0, 1.4, 2.0, 2.8, 4.0, 5.7, 8.0, 11.3, 16.0, 22.6, 32.0, 45.3, 64.0, 90.5, 128.0
r_e	Effective radius	μm	5.0, 6.3, 7.8, 9.6, 11.6, 13.8, 16.3, 19.1, 22.2, 25.7, 29.4, 33.6, 38.1, 42.9, 48.2, 53.9, 60.0
$ICOTF$	$\tau_{ICE}/(\tau_{LIQ} + \tau_{ICE})$	-	0, 0.125, 0.25, 0.375, 0.5, 0.625, 0.75, 0.875, 1
TPW	Total precipitable water for H_2O	mm	[0.000, 0.001, 0.004, 0.01, 0.02, 0.04, 0.1, 0.2, 0.4, 0.8, 1, 2, 3, 4, 6, 8] + [10, …, 100 by 5]
COL	Column mean concentration for CO_2	ppmv	350, …, 450 by 10
DU	Dobson unit of O_3	DU	100, …, 500 by 50

Text S2. Sensitivity analysis

A sensitivity analysis was performed based on the error propagation theory using radiative transfer calculations, as described below:

[Figure S1]

Figure S1 illustrates how measurement errors in each SGLI observation channel propagate to the retrieval errors of cloud properties. These retrieval errors were calculated using the following formula:

$$\Delta \boldsymbol{x} = (\boldsymbol{K}^T \boldsymbol{K})^{-1} \boldsymbol{K}^T \Delta \boldsymbol{y}, \quad (S10)$$

where $\Delta \boldsymbol{y}$, $\Delta \boldsymbol{x}$, and $\boldsymbol{K}$ represent the measurement error, the retrieval error, and the Jacobian matrix of the forward model $\boldsymbol{F}(\boldsymbol{x})$ evaluated at the state vector $\boldsymbol{x}$, respectively. For the calculations in Figure S1, $\boldsymbol{y} = (R_{\mathrm{SW1}}, R_{\mathrm{SW4}}, R_{\mathrm{SW3}}, I_{\mathrm{TI1}}, R_{\mathrm{VN9}})^T$ and $\boldsymbol{x} = (COT, CER, ICOTF, CTH, CBH)^T$, where R_λ and I_λ are the measured TOA reflectance and radiances at the SGLI channels λ, respectively. Note that, for clarity, these elements of $\boldsymbol{y}$ were limited to five channels with significant sensitivity to each element of $\boldsymbol{x}$. Perturbations ranging from -2% to +2% were applied to the measured values of each channel, and retrieval errors were calculated using equation (S10). This process was repeated for all channels.

[Figure S2]

Second, Figure S2 illustrates how the overall uncertainties in SGLI observations used in inverse estimation propagate to the uncertainty in the estimation.

$$\boldsymbol{S}_x = (\boldsymbol{K}^T \boldsymbol{S}_e^{-1} \boldsymbol{K})^{-1}, \quad (S11)$$

where $\boldsymbol{S_e}$ and $\boldsymbol{S_x}$ represent the covariance matrices for the measurement vector $\boldsymbol{y}$ and the state vector $\boldsymbol{x}$, respectively, indicating the uncertainties in the measurements and retrievals. As the measurement uncertainty, standard deviations corresponding to 0% to 2% of the measured values were assigned to the diagonal elements of $\boldsymbol{S_e}$, and the retrieval uncertainty $\boldsymbol{S_x}$ was calculated using equation (S11).

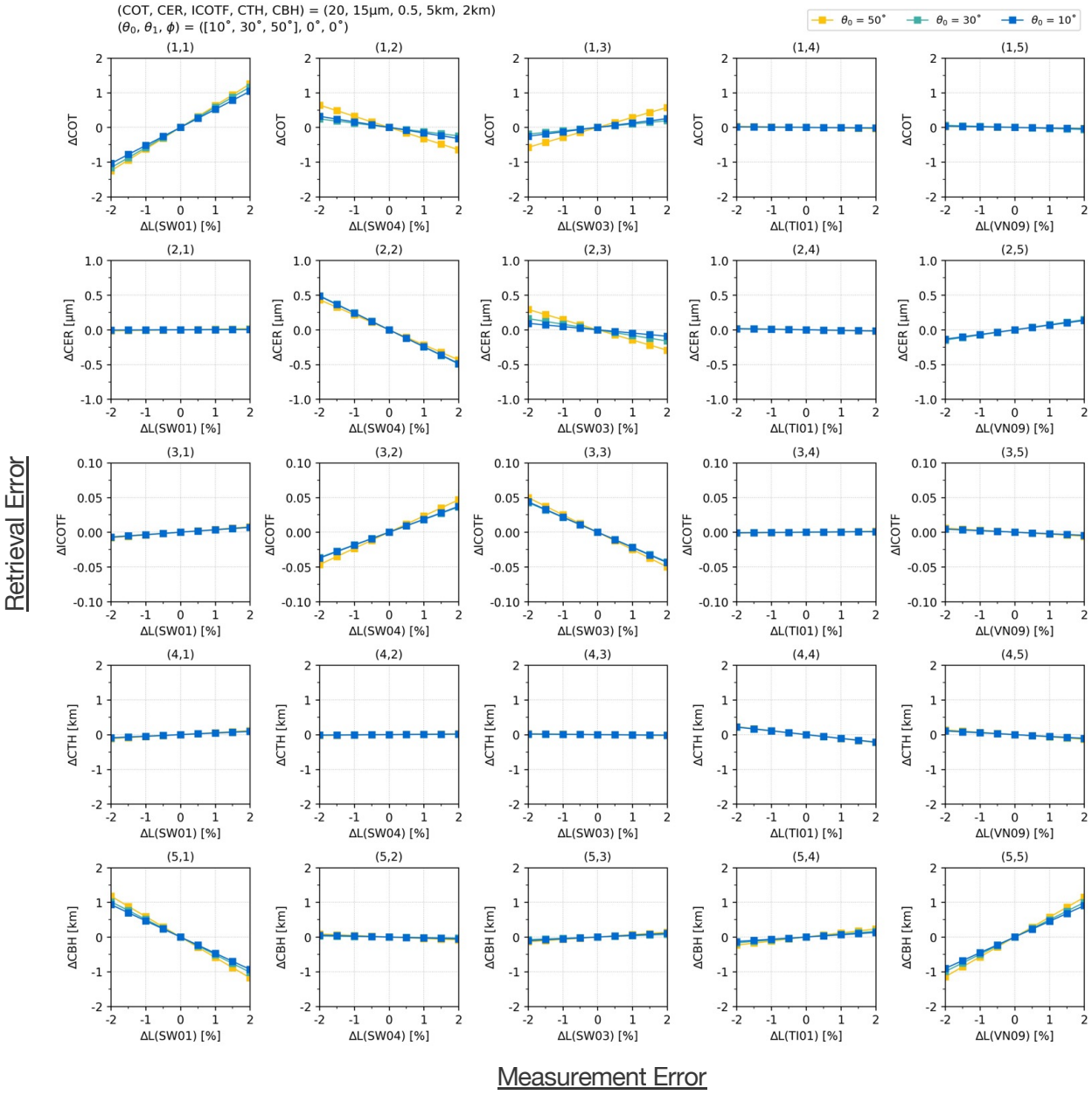

Figure S1 Impact of measurement errors on retrieval errors. Horizontal panels correspond to SGLI channels where measurement errors are introduced, while vertical panels correspond to cloud properties being retrieved. In each panel, the x-axis represents the relative error in radiance, and the y-axis represents the corresponding retrieval error. SW1, SW4, SW3, TI1, and VN9 are SGLI spectral channels centered at 1.05 μm, 2.21 μm, 1.63 μm, 10.8 μm, and 763 nm, respectively. COT, cloud optical thickness; CER, cloud effective radius; ICOTF, ice COT fraction; CTH, cloud top height; CBH cloud base height; θ_0, solar zenith angle; θ_1, sensor zenith angle;ϕ, relative azimuth angle.

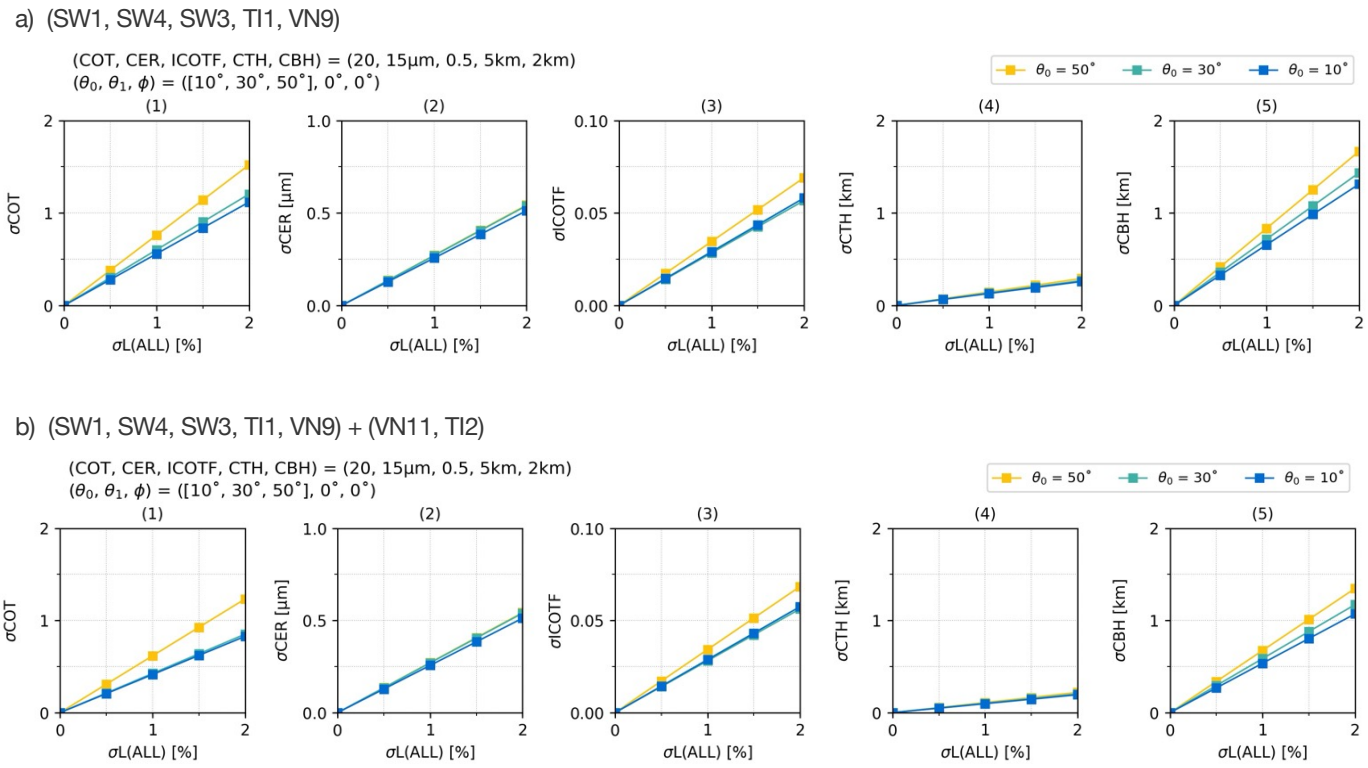

Figure S2. Retrieval uncertainty due to measurement uncertainty, calculated using equation (S11), and its dependence on the combinations of channels used for retrieval. a) Use SW1, SW4, SW3, TI1, and VN9; b) Adding VN11 and TI2 to the channels in a). The $\boldsymbol{\sigma L}$ on the x-axis represents the uncertainty in radiance (standard deviation) assigned to the diagonal elements of $\boldsymbol{S_e}$ in equation (S11), assuming the same relative error for all channels. The y-axis corresponds to the uncertainty (standard deviation) in the retrieval, derived from the diagonal elements of $\boldsymbol{S_x}$. SW1, SW4, SW3, TI1, and VN9 are SGLI spectral channels centered at 1.05 μm, 2.21 μm, 1.63 μm, 10.8 μm, and 763 nm, respectively. COT, cloud optical thickness; CER, cloud effective radius; ICOTF, ice COT fraction; CTH, cloud top height; CBH cloud base height; θ_0, solar zenith angle; θ_1, sensor zenith angle;ϕ, relative azimuth angle.

Other supplemental figures

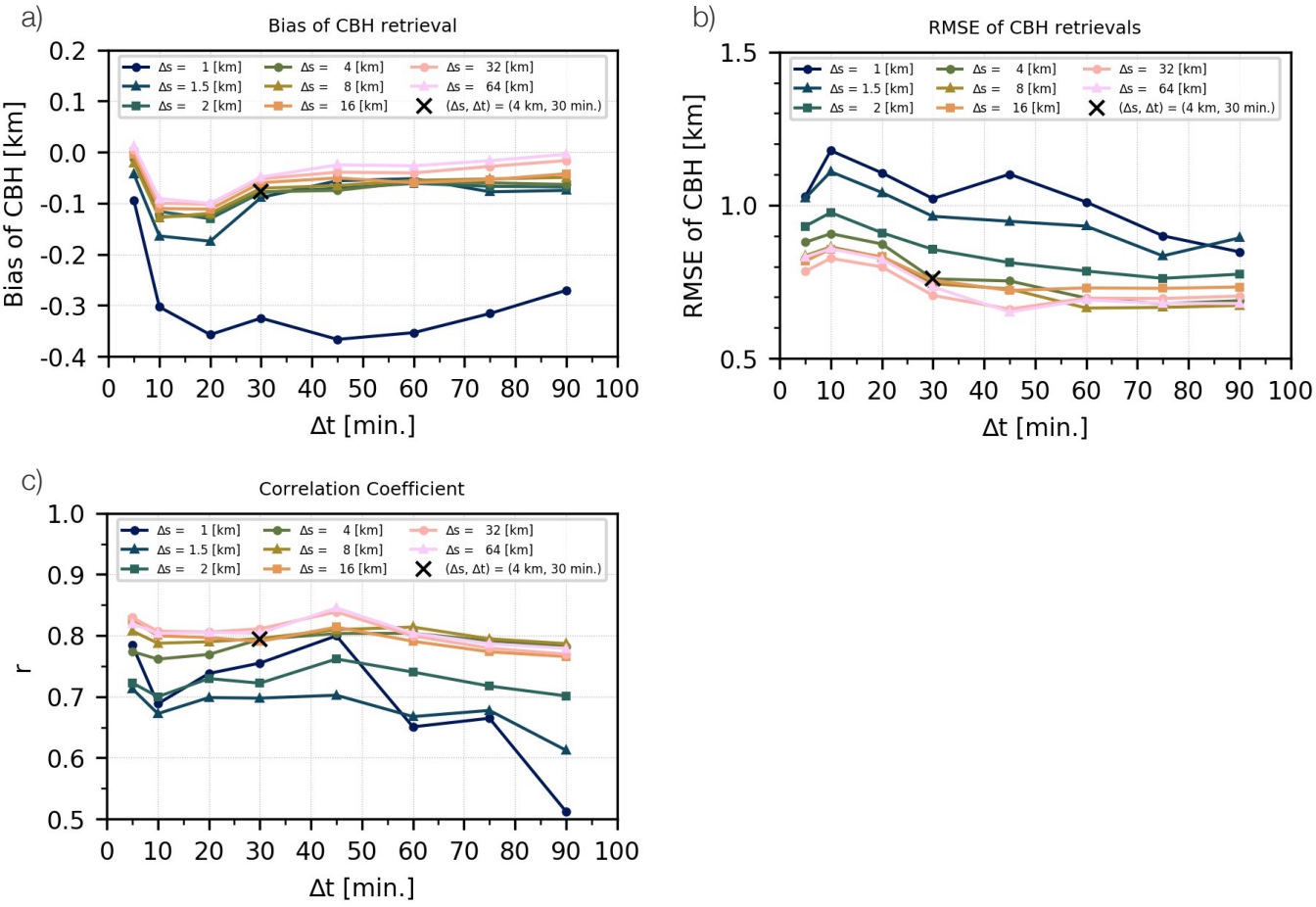

Figure S3. Spatial and temporal dependence of a) bias, b) root mean square error (RMSE), and c) correlation coefficient (r) between cloud base height (CBH) derived from the GCOM-C/SGLI and the EUMETNET E-profile ceilometer observations; Δs represents the distance from the site used for averaging the SGLI CBH, Δt represents the time window used for averaging the ceilometer CBH, and the x-mark correspond to the Δs and Δt values used in Figure 6.

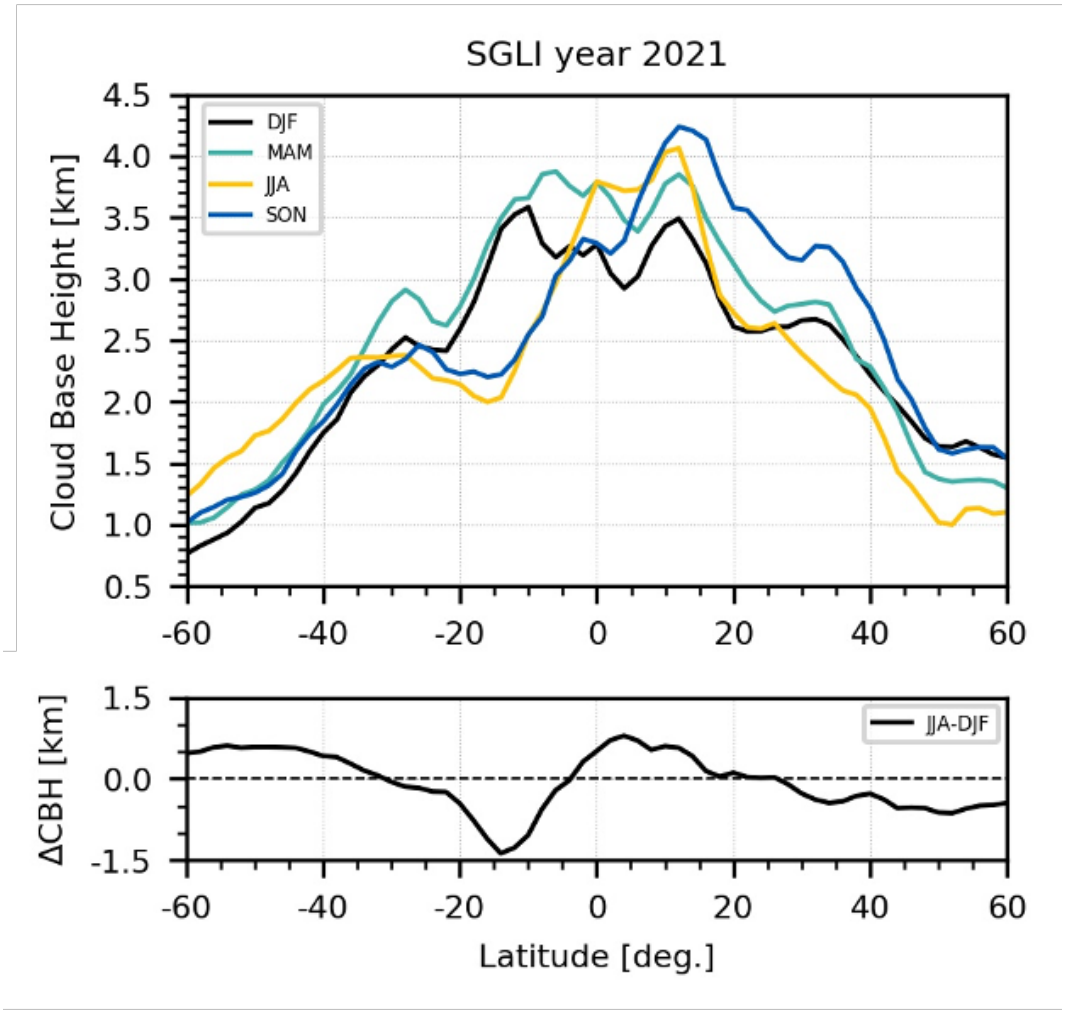

Figure S4. Seasonal variation of the zonal mean cloud base height (top) and the difference between the JJA and DJF months (bottom).

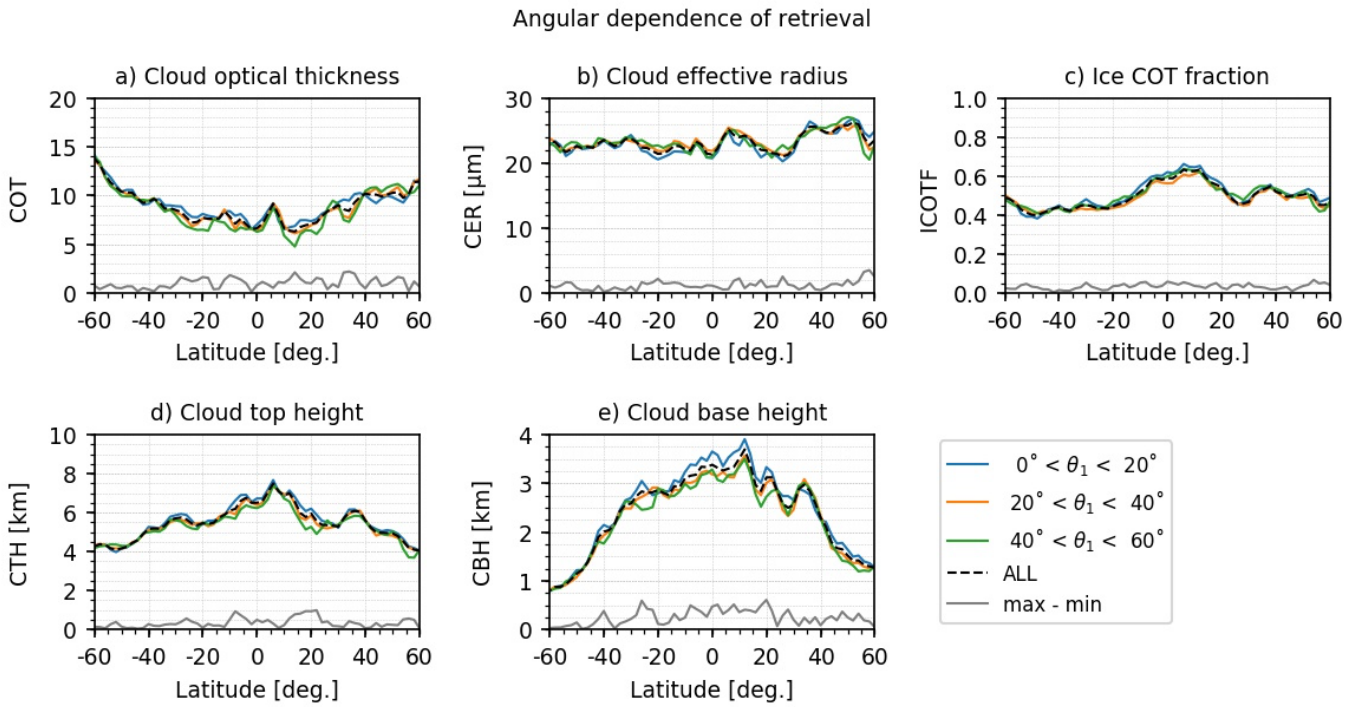

Figure S5. Angular dependence of cloud property retrieval. Zonal means of a) cloud optical thickness (COT), b) cloud effective radius (CER), c) ice COT fraction (ICOTF), d) cloud top height (CTH), and e) cloud base height (CBH), categorized by different ranges of satellite zenith angle (θ_1).

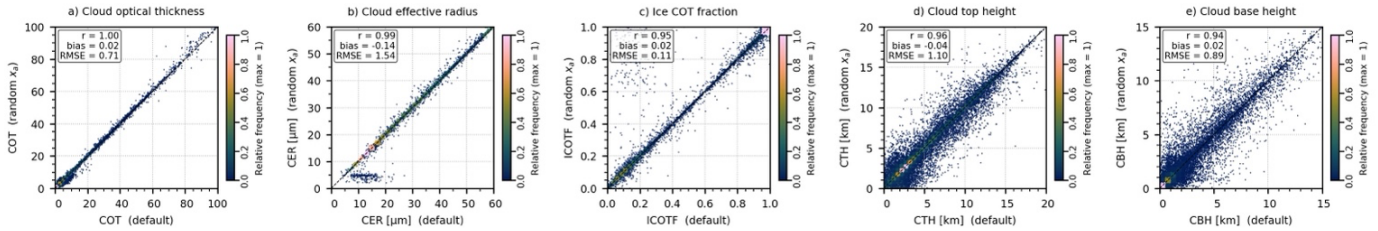

Figure S6. Dependence on $\boldsymbol{x_a}$ for cloud retrieval. The x-axis represents the cloud retrieval obtained under the same settings (i.e., default) as specified in Table 1 of the main text, while the y-axis represents the cloud retrieval obtained when the elements of $\boldsymbol{x_a}$ were assigned random numbers following uniform distributions within the range defined in Table 1. COT, cloud optical thickness; CER, cloud effective radius; ICOTF, ice COT fraction; CTH, cloud top height; CBH cloud base height.

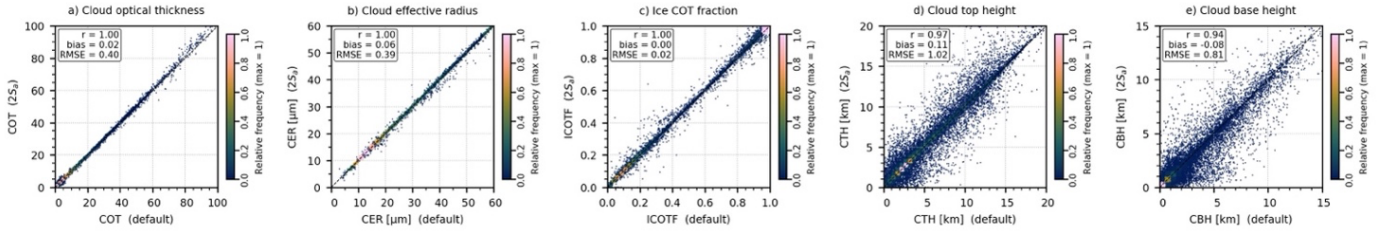

Figure S7. Dependence on $\boldsymbol{S_a}$ for cloud retrieval. Same as Figure S6, except the y-axis represents the cloud retrieval obtained under a relaxed priori distribution of $2\boldsymbol{S_a}$.

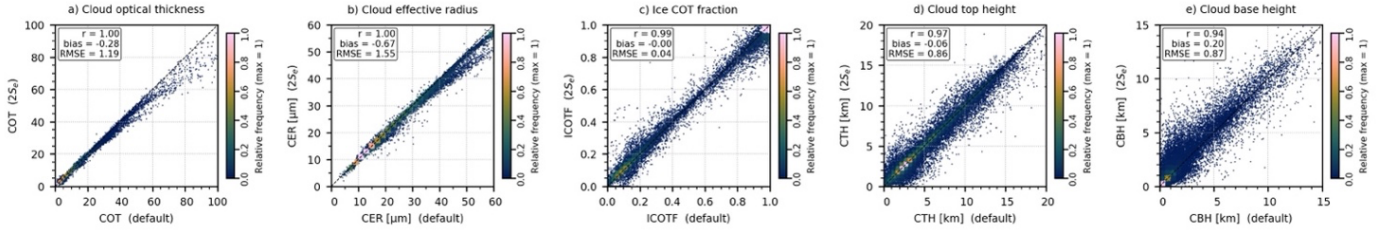

Figure S8. Dependence on $\boldsymbol{S_e}$ for cloud retrieval. Same as Figure S6, except the y-axis represents the cloud retrievals obtained under an increased measurement uncertainty of $2\boldsymbol{S_e}$.